Comparison between laboratory and airborne BRDF measurements for remote sensing

Georgi T. Georgiev[a], Charles K. Gatebe[b], James J. Butler[c], Michael D. King[c]

[a]Science Systems and Applications, Inc., Lanham, MD 20706, e-mail: ggeorgi@pop900.gsfc.nasa.gov

[b]Goddard Earth Science and Technology Center, University of Maryland Baltimore County, Baltimore, MD 21228

[c]Earth-Sun Exploration Division, NASA Goddard Space Flight Center, Greenbelt, MD 20771

ABSTRACT

Samples from soil and leaf litter were obtained at a site located in the savanna biome of South Africa (Skukuza; 25.0°S, 31.5°E) and their bidirectional reflectance distribution functions (BRDF) were measured using the out-of-plane scatterometer located in the National Aeronautics and Space Administration's (NASA's) Goddard Space Flight Center (GSFC) Diffuser Calibration Facility (DCaF). BRDF was measured using P and S incident polarized light over a range of incident and scatter angles. A monochromator-based broadband light source was used in the ultraviolet (uv) and visible (vis) spectral ranges. The diffuse scattered light was collected using an uv-enhanced silicon photodiode detector with output fed to a computer-controlled lock-in amplifier. Typical measurement uncertainties of the reported laboratory BRDF measurements are found to be less than 1% (k=1). These laboratory results were compared with airborne measurements of BRDF from NASA's Cloud Absorption Radiometer (CAR) instrument over the same general site where the samples were obtained. This study presents preliminary results of the comparison between these laboratory and airborne BRDF measurements and identifies areas for future laboratory and airborne BRDF measurements. This paper presents initial results in a study to try to understand BRDF measurements from laboratory, airborne, and satellite measurements in an attempt to improve the consistency of remote sensing models.

Keywords: Remote sensing, Optical scattering, BRDF, Reflectance spectroscopy.

1. INTRODUCTION

The monitoring of land surface is a major science objective in Earth remote sensing. A major goal is to identify major biomes and to map and distinguish the changes in their composition introduced by anthropogenic and climatic factors. Currently, deforestation and desertification are the most important land cover area processes of scientific interest. These processes play a major role in climate variation particularly with respect to clouds and rainfall. Given known anthropogenic influences on climate, air, and water quality, biome mapping has clearly become a research priority. Understanding the spatial characteristics of the properties of biomes will help in the formulation of site-specific management plans over the globe. Changes in the chemistry and dynamics of land and sea are directly connected with Earth geophysical processes, which include the circulation of the major air and sea currents, the type, concentration and distribution of atmospheric aerosols, and the formation of clouds. The modeling of the processes at work will help predict the changes in major Earth biomes and their impact on climate variation.

The BRDF of a sample describes the spatial and spectral energetic interaction of light on that sample's surface as a function of the incident and scatter angles and wavelength. It is used in modern optical engineering to characterize the spectral and geometrical optical scatter of both diffuse and specular samples. The BRDF is particularly important in the characterization of reflective and transmissive diffusers used in the pre-flight and on-orbit radiance and reflectance calibrations of Earth remote sensing instruments. Satellite BRDF measurements of Earth scenes can be used as a

Earth Observing Systems XI, edited by James J. Butler, Jack Xiong,
Proc. of SPIE Vol. 6296, 629603, (2006) · 0277-786X/06/$15 · doi: 10.1117/12.680542

sensitive tool for early detection of changes occurring in vegetation canopies, soils, or the oceans. For example, water content changes in soil and vegetation can be detected and monitored using BRDF.

Significant efforts have been invested in the study of the Earth's major biomes. At NASA's Goddard Space Flight Center, King et al. [1], have developed an airborne, multi-wavelength scanning Cloud Absorption Radiometer (CAR). CAR is a scanning radiometer designed to scan from 5^o before zenith to 5^o past nadir, corresponding to a total scan range of 190^o. The instrument scan track extends from nadir up to 95^o of the aircraft direction. CAR's 14 channels are located between 340 and 2301 nm. They were selected to avoid the molecular absorption bands in the near and shortwave infrared. The first 8 channels between 340 and 1270 nm are simultaneously and continuously sampled, while the ninth registered channel is selected from the six remaining channels between 1550 and 2301 nm.

The CAR instrument has flown in many national and international field experiments. For example, CAR was used to study the directional and spectral reflectance of Kuwaiti oil-fire smoke in 1992, King[2]. The angular reflectance pattern was measured at 13 wavelengths between 0.5 and 2.3 μm. The reflectance of the smoke layer was found to be 12% in the nadir direction. The observations revealed a backscattering maximum in the antisolar direction and enhanced scattering near the rainbow direction. Those characteristics indicated that the smoke layer 90 km downwind was composed of oil drizzle droplets that scatter solar radiation as a layer composed of spherical particles.

Gatebe at al.[3] studied the ocean directional reflectance using the CAR instrument. The Cloud Absorption Radiometer (CAR) was flown over the Atlantic Ocean off the eastern seaboard of the United States in the vicinity of the Chesapeake Light Tower and over nearby National Oceanic and Atmospheric Administration (NOAA) buoy stations and obtained BRDF measurements of the Ocean with solar zenith angles from 15^o to 46^o. The method of spherical harmonics with a Cox-Munk distribution was used to develop a new algorithm to solve the atmosphere-ocean radiative transfer problem and to filter the effects of the atmosphere in airborne measurements. This algorithm simultaneously retrieved the wind speed and full ocean BRDF from CAR measurements and evaluated the total and equivalent albedos.

Using data from CAR, Arnold et al.[4] presented the BRDF for four common arctic surfaces: snow-covered sea ice, melt-season sea ice, snow-covered tundra, and tundra shortly after snowmelt. The BRDF was observed to be higher for snow-covered sea ice than melt season sea ice at all wavelengths between 470 nm and 2300 nm with the difference increasing with wavelength. The BRDF of snow-covered tundra was observed to be higher than for snow-free tundra at wavelengths less than 1640 nm with the difference decreasing with wavelength.

Relevant to the study outlined in this paper, Gatebe et al.[5] obtained BRDF data on ecosystems in southern Africa using the CAR instrument. The validation sites included Skukuza tower, South Africa, and Mongu towers, Zambia. The results show an anisotropy in reflected solar radiation depending on surface type. The greatest anisotropy was observed over marine stratus clouds exhibiting strong forward scattering. A distinct backscattering peak in the principal plane characterized the BRDF over savanna. The BRDF over pans was more enhanced in the backscattering plane and showed little directional variation.

The BRDF of well-defined spectrally flat surfaces such as Spectralon has been extensively studied[6] and models have been developed for its prediction. BRDF models can be classified as numerical or analytical. Numerical models deal with the surface geometry[7] using ray tracing techniques and/or Monte-Carlo methods. The analytical models are theoretical – build formulas describing BRDF[8], or empirical – based on empiric parameters. Some of the models concentrate on modeling remote sensing objects such as vegetation surfaces[9]. Others are more oriented to modeling the BRDF of laboratory samples used for the calibration of remote sensing instruments. These can also be classified as models of plain surfaces and models of structured surfaces. BRDF models are widely used in computer design, the graphics industry, Earth remote sensing, and planetary studies.

In this study, we examine the correlation between laboratory measurements of biome soil and leaf samples and in-situ airborne BRDF measurements while trying to understand the roles of spatial and spectral variability of the natural biome and accounting for atmospheric scattering and radiometric transfer. The samples measured in the laboratory included leaf litter, predominantly from acacia trees, and two different composition soils, all collected from the savanna biome of Skukuza, South Africa. Their BRDF was measured using the scatterometer located in the Diffuser Calibration Facility (DCaF) of NASA's Goddard Space Flight Center. The samples were measured at both in-plane and out-of-plane geometries and at a number of incident angles and wavelengths. The light source used in the laboratory BRDF measurements was a short-arc Xenon lamp - monochromator assembly producing an incoherent, tunable light source

with a well-defined spectral bandpass. The accuracy of measured BRDF depended on the signal-to-noise ratio and was determined by a sample's spatial optical scatter properties. The scatterometer can perform in-plane and out-of-plane bidirectional reflectance distribution function (BRDF) and bidirectional transmission distribution function (BTDF) measurements with typical measurement uncertainties of 1 % (k = 1), where k is the coverage factor or better. The results presented here are traceable to the National Institute of Standards and Technology's (NIST's) Special Tri-function Automated Reference Reflectometer (STARR)[10]. The initial results of comparing lab and airborne BRDF measurements presented in this paper have identified the need for future, additional lab BRDF measurements on natural samples.

2. METHODOLOGY

The term *reflectance* is usually used to describe the diffuse scattering of light in arbitrary directions by a geometrically complex medium. The *reflectance* is additionally specified by two adjectives describing the degree of collimation of the source and detector, according to Nicodemus et al.[11]. The directional-hemispherical reflectance is the total fraction of light scattered into hemisphere by illumination with a collimated source surface. The bidirectional reflectance corresponds to directional-directional reflectance and ideally means both incident and scattered light beams are collimated. Although perfect collimation and diffuseness are rarely achieved in practice, they can be used as very useful approximations for reflectance measurements.

We are following the NIST definition of BRDF, according to Nicodemus, in our laboratory calibration measurements. In this case, the BRDF is referred to as the ratio of the scattered radiance, L_s, scattered by a surface into the direction (θ_s, ϕ_s) to the collimated irradiance, E_i, incident on a unit area of the surface:

$$BRDF_N = \frac{L_s(\theta_i, \phi_i, \theta_s, \phi_s, \lambda)}{E_i(\theta_i, \phi_i, \lambda)}, \tag{1}$$

where the N subscript denotes BRDF after Nicodemus, θ is the zenith angle, ϕ is the azimuth angle, the subscripts i and s represent incident and scattered directions, respectively, and λ is the wavelength. In the laboratory, we usually describe $BRDF_N$ in terms of the incident power, the scattered power and the geometry of the reflected scatter. It is equal to the scattered power per unit solid angle normalized by the incident power and the cosine of the detector view angle[12], Fig.1:

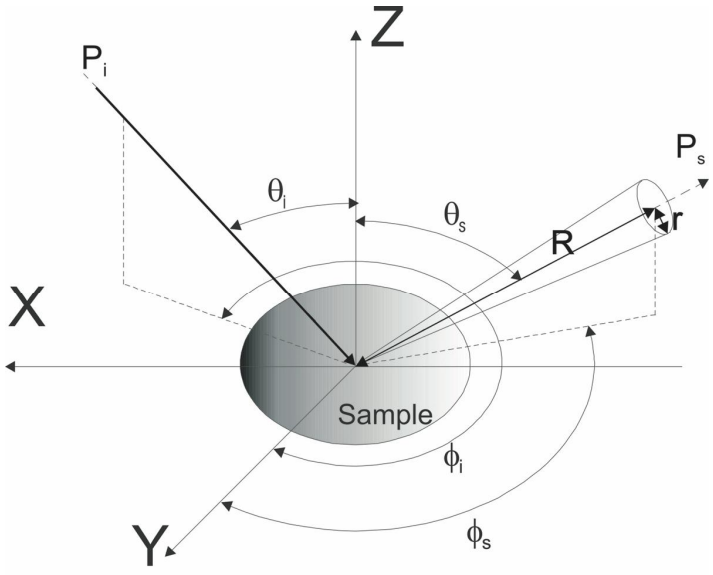

Fig.1: BRDF after Nicodemus.

$$BRDF_N = \frac{P_s / \Omega}{P_i \cos\theta_s}, \tag{2}$$

where P_s is the scatter power, Ω is the solid angle determined by the detector aperture, A, and the radius from the sample to the detector, R, or $\Omega = A/R^2$, P_i is the incident power, and θ_s is the scatter zenith angle.

BRDF has units of inverse steradians and can range from very small numbers (e.g. off-specular black samples) to very large values (e.g. highly reflective samples at specular reflectance).

3. MEASUREMENTS

The NASA's DCaF scatterometer seen in Fig.2 was used to measure the BRDF at different source and detector angular configurations. More detailed information on the scatterometer is published elsewhere[13]. The samples were two types of soil and dry crushed leaf litter mainly from acacia trees and grass. The samples were taken from the savanna biome of Skukuza, South Africa, Fig.3. They were placed in square 50 x 50 x 5 mm black plastic holders with the

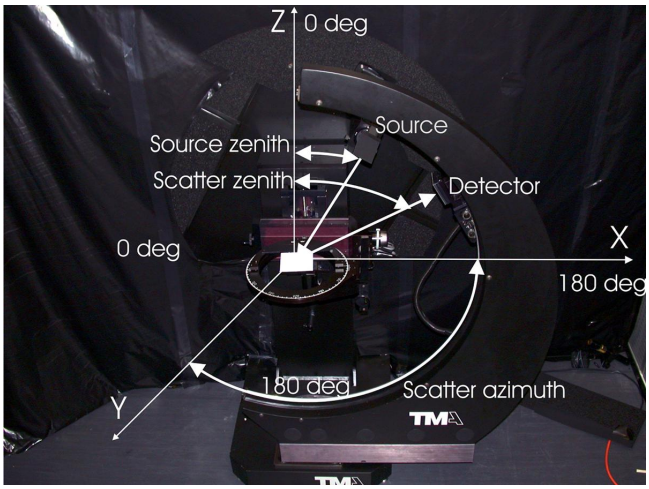

Fig. 2: The Scatterometer

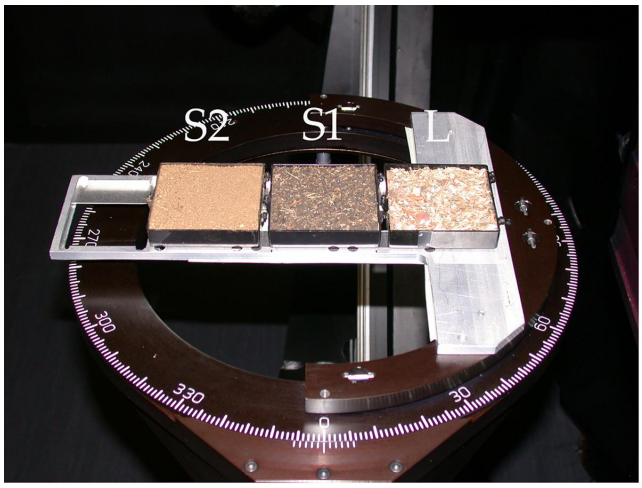

Fig.3: The samples

sample surface well flattened and uniform particles distribution through the entire surface area. The holders were then mounted horizontally on the sample stage and aligned with the scatterometer axes of rotation. The sample stage can be moved in the X, Y and Z linear directions using three motor stages. There is also an additional degree of freedom allowing sample rotation in the horizontal plane. The detector field-of-view was centered on each sample target for all measurements and was under filled by the incident beam. The incoherent, monochromator-based light source was a 75 W Xenon lamp coupled to a Chromex 0.25m monochromator with a spectral bandwidth of 12 nm. Scattered light was detected using a polarization insensitive detector employing an ultraviolet enhanced silicon photodiode with output fed to a computer-controlled lock-in amplifier. The position of the detector assembly is described by the scatter zenith and scatter azimuth angles. The detector assembly can be rotated around the vertical and horizontal axes of the goniometer. Using the motor sample stages the surface of the sample to be measured was positioned at the cross point of the two perpendicular goniometer rotation axes which define the center of rotation of the goniometer system. All measurements were made for polarizations of the illumination beam both parallel, P, and perpendicular, S, to the plane of incidence. The BRDF, for each polarization was calculated by dividing the net signal from the transmitted radiant flux by the incident flux and the projected solid angle from the calibration item to the limiting aperture of the detector. This setup facilitates the acquisition of computerized BRDF measurements at different incident and scattered geometries for a complete data acquisition at selected points and wavelengths. The measurement uncertainty, Δ_{BRDF}, depends on several instrument variables. It was consequently evaluated in accordance with NIST guidelines[14] to be less than 1% (k=1). The facility has participated in several round-robin measurement campaigns with domestic and foreign calibration institutions in support of Earth and space satellite validation programs[15]. BRDF at different directions, backscatter, reciprocity and 8^o directional/hemispherical reflection of similar to the current soil samples regolith simulant was already characterized at the facility[16].

4. RESULTS AND DISCUSSION

To properly characterize the samples, we recorded data at incident angles of 0^o, 30^o, and 60^o. The detector was positioned at scatter zenith angles of 0^o to 60^o with data acquired in steps of 5^o. The wavelengths were 340 nm, 470 nm and 870 nm.

4.1. BRDF at normal incidence

The in-plane BRDF for the three samples is shown in Figs.4, 5, and 6 for 340, 470 and 870 nm, respectively. The wavelength dependence of BRDF is given in Fig.7, where the detector was fixed at 30^o scatter zenith angle.

The BRDF increases with increasing wavelength and scatter zenith angles for all samples. Some noise is visible in the 340 nm data where the BRDF is between 0.007 and 0.017 sr^{-1}.

4.2. BRDF at non-normal incidence

The BRDF at non-normal incidence angles of 30^o and 60^o are shown in Figs. 8 through 13 at wavelengths of 340, 470 and 870 nm. The lowest values of BRDF are seen in the 340 nm data. The shapes of the BRDF curves depend strongly on the nature of the sample (i.e. soil versus leaf) and the angle of incidence. In all the figures, the soil samples, S1 and S2, exhibit enhanced back scattering properties when the backscatter is presented by simply taking the difference of the BRDF at scatter angles symmetric to the sample normal. This is seen in the higher BRDF measurements at negative scatter zenith angles relative to those made at positive scatter zenith angles. The leaf litter sample, L, however, behaves differently. At 30^o angle of incidence, the L sample exhibits enhanced forward scattering at 340 and 470 nm (i.e. Figs. 8 and 9) and enhanced backscattering at 870 nm (i.e. Fig. 10). At 60 ° angle of incidence, the L sample exhibits enhanced forward scattering at 340 nm (i.e. Fig. 11) and enhanced backscattering at 470 and 870 nm (i.e. Figs. 12 and 13). The enhanced backscattering in the L sample is seen to increase with increasing wavelength. Although it could not be measured due to the relative geometries of the scatterometer optics and detector, the BRDF for all samples show

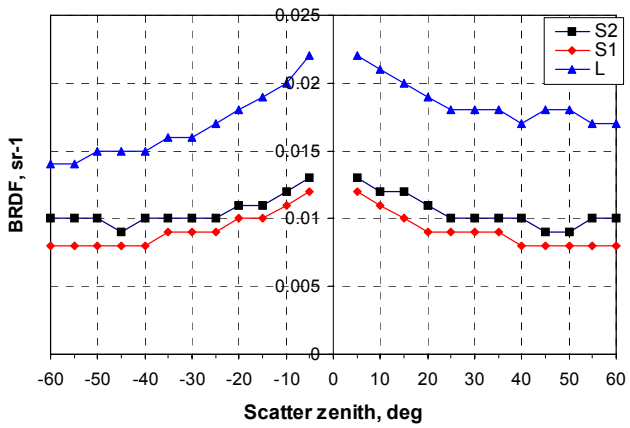

Fig.4: BRDF at normal incidence, 340 nm

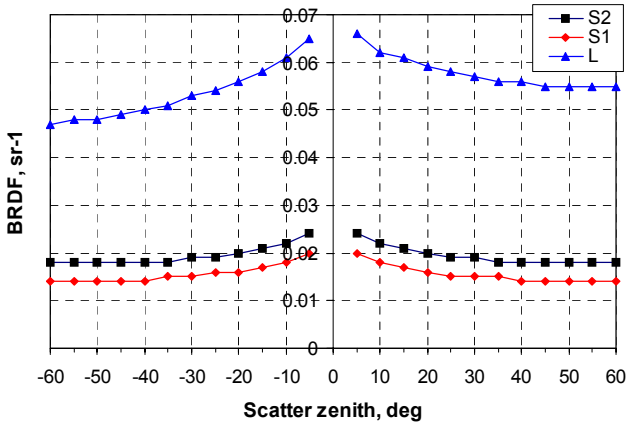

Fig.5: BRDF at normal incidence, 470 nm

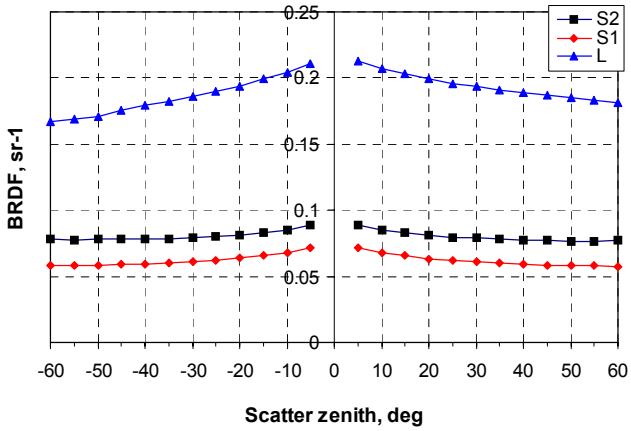

Fig.6: BRDF at normal incidence, 870 nm

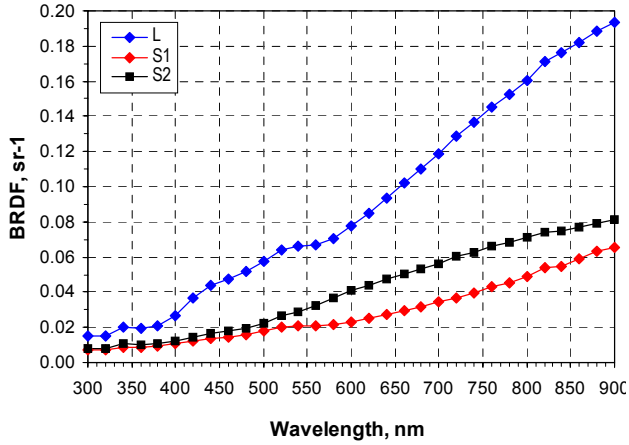

Fig.7: BRDF wavelength dependence

evidence of a significant opposition effect represented by increased light being retroscattered back in the direction of the incident beam.

4.3. BRDF from airborne measurements

The CAR instrument, as depicted schematically in Fig.14, was used for airborne BRDF measurements of the savanna biome of South Africa (Skukuza; 25.0°S, 31.5°E) shown in Fig.15. The main characteristics of the CAR instrument include:

- 14 spectral bands: 0.34 to 2.29 µm
- scan range: ±95° from horizon on right-hand side of aircraft
- field of view: 17.5 mrad (1°)
- scan rate: 1.67 Hz (100 rpm)
- data system: 9 channels @ 16 bit
- 382 pixels in scan line

The BRDF from a vegetation rich surface recorded over Skukuza in August 2000 is shown in Fig.16 for scatter angles from –80° to 80° and for wavelengths of 470 nm, 870 nm and 1036 nm. The incident light angle was -67°. A second simulation of satellite signal in the solar spectrum (6S) model was used[17]. A hot spot or retroscatter signal is seen

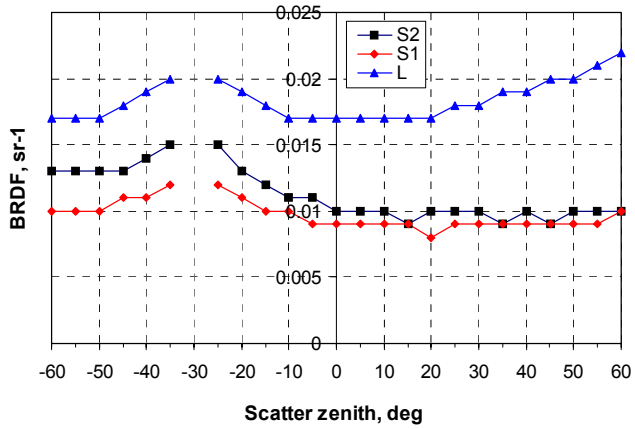

Fig.8: BRDF at 30 deg incidence, 340 nm

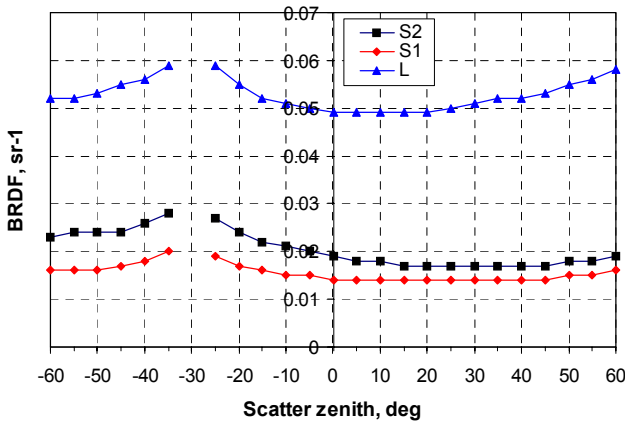

Fig.9: BRDF at 30 deg incidence, 470 nm

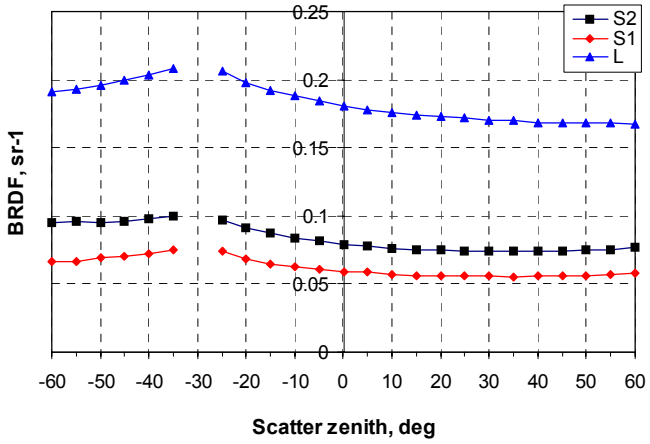

Fig.10: BRDF at 30 deg incidence, 870 nm

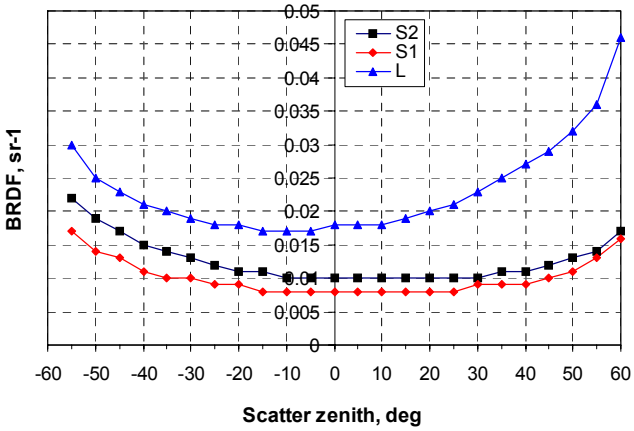

Fig.11: BRDF at 60 deg incidence, 340 nm

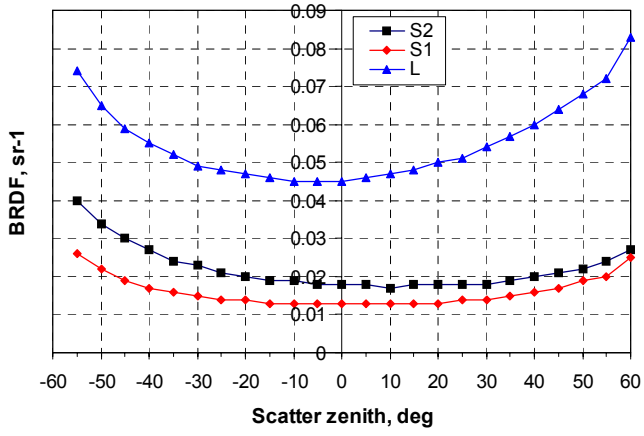

Fig.12: BRDF at 60 deg incidence, 470 nm

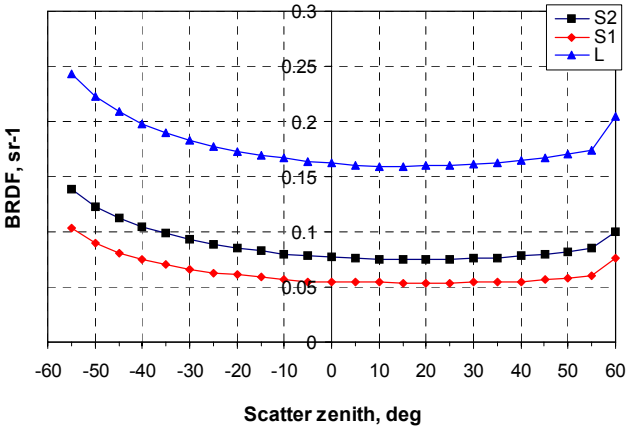

Fig.13: BRDF at 60 deg incidence, 870 nm

at -70^{o}. The airborne-recorded BRDF shows backscattering properties of the vegetation covered soil surface. The BRDF increases with wavelength.

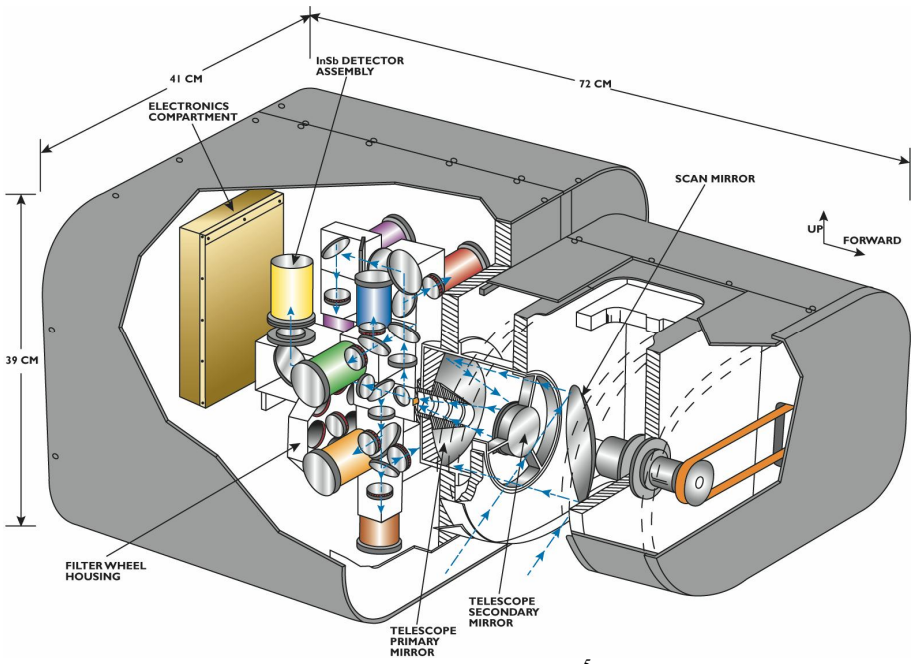

Fig.14: CAR instrument[5]

Both the Lab and airborne BRDF data measured at 470 nm and 870 nm are shown in Fig.17. The lab curves in Fig.17 were generated assuming 90% vegetation cover and 10% exposed soil determined by the field campaign participants. The same general shape of the BRDF curves is reproduced by the lab and airborne measurements. The BRDF at 470 nm matches well. However there is a significant deviation between the lab and airborne data at 870 nm particularly at increasingly negative scatter angles. At high negative scatter angles, the lab data is lower than the airborne data. In an effort to understand this difference, the BRDF of fresh vegetation was compared to that of dried vegetation using lab measurements of each using the scatterometer. One proposed explanation for part of this BRDF difference could be attributed to different fractions of living to dried, dead vegetation leading to the observed optical scatter differences. To examine this possibility, the BRDF of fresh and dry tuliptree (*Liriodendron Tulipifera*) leaves was measured in the lab. We still need to compare the acacia and tuliptree leaves BRDF with Lab measurements but based on their surface structure and chlorophyll content we do believe the BRDF of the two species is very close. These results are shown in Fig.18 for 300 nm, 500 nm, and 900 nm at a 30^o incident angle.

Although the data of Fig.18 were measured only at a -30^o incident angle and not at -67°, it shows that dry and fresh leaf samples exhibit different BRDF curve shapes. The dry leaves have lower BRDF at smaller scatter angles compared to the fresh leaves and higher BRDF in the forward scatter direction. Conversely, fresh leaves exhibit a relatively flat BRDF with a slight decrease toward higher forward scatter angles. For all wavelengths, the BRDF of fresh leaves at low scatter angles is higher than that for dried leaves. At 42^o scatter angle for 900 nm, 49^o for 500 nm, and 58^o for 300 nm, the BRDF of dry and fresh leaves is identical. The dependence of the shape of the BRDF curve on the degree of senescence of the vegetation is one of several possible reasons for the differences between the CAR and lab measurements at 870 nm. The identification of this and other sources for differences in lab and airborne BRDF measurements through quantification of their effects on measured BRDF is an on-going goal of this research.

5. CONCLUSIONS

Laboratory BRDF measurements of three samples from Skukuza biome in South Africa are presented in this paper. One of the samples is dry leaf litter; the other two are different soils. The samples were measured at illumination of 0^o, 30^o, and 60^o. The scatter angles were from 0^o to 60^o in steps of 5^o. The wavelengths were 340 nm, 470 nm, and 870

Fig.15: Skukuza, South Africa

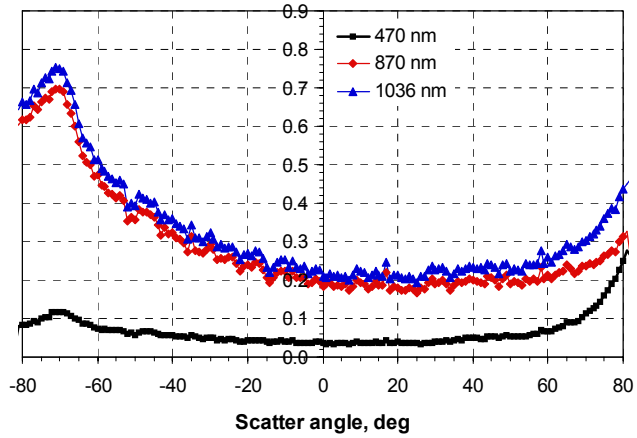

Fig.16: Airborne data, 67 deg incident angle

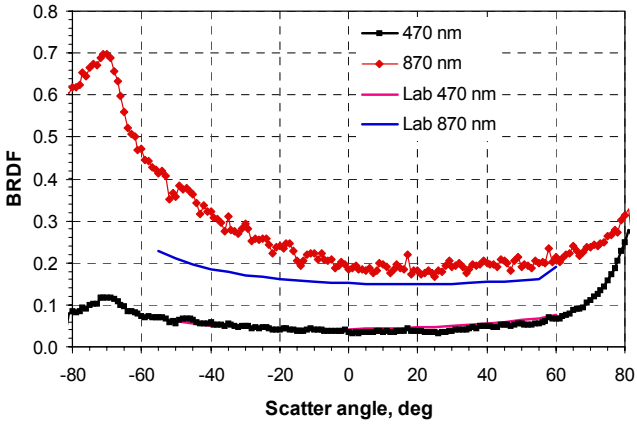

Fig.17: Airborne -67 deg to Lab 60 deg incident angle

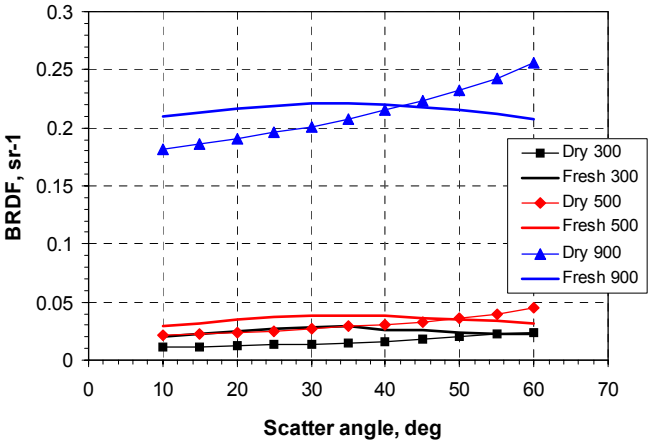

Fig.18: Fresh and Dry White Oak leaves at -30 deg incident angle, 300nm, 500nm, 900nm

nm. The samples were measured at the Diffuser Calibration Facility of NASA's GSFC using the facility's scatterometer. A broadband xenon-arc coupled to a monochromator light source was used. It was found that the BRDF for all three samples increases with wavelength. At incident angles of 30° and 60°, the soil samples demonstrate enhanced backscattering. The leaf litter sample backscatters at 870 nm but it has a forward scatter at 340 and 470 nm. The forward and backward scatters are better pronounced at 60° incident angle.

Airborne BRDF measurements were performed over Skukuza, South Africa during the dry season of 2000 using the CAR instrument. BRDF data at -67° incident angle, scatter angles from –80° to 80°, wavelengths of 470 nm, 870 nm, and 1036 nm are presented. The airborne BRDF shows that the optical backscattering of the observed surface increases with the wavelength. Lab and airborne data sets were compared at 470 nm and 870 nm, at 60° incident angle for the lab, and at 67° incident angle for the airborne instrument. The BRDF at 470 nm matched well. However there is a discrepancy between lab and airborne data at 870 nm particularly at backscatter angles from –55° to 0°. We examined the difference between the optical scattering properties of fresh and dried vegetation in an effort to identify one possible source for this difference. The spectral dependence of BRDF on the freshness of the vegetation was studied by measuring the BRDF of fresh and dry tuliptree leaves in the lab at 300 nm, 500 nm, and 900 nm and at a 30° incident angle. Dried leaves exhibited lower BRDF values at small scatter angles compared to fresh leaves. At large scatter

angles, the fresh leaves exhibited a lower BRDF. The degree of senescence of vegetation is one potential source of the difference between the lab and airborne measurements.

We would like to address in the future the different BRDF calculation at Lab – Nicodemus and at airborne – van de Hulst, the difference contributed to the angles of incidence, to explore our long-term goal - the potential of airborne and laboratory multispectral and multiangular measurements in satellite remote sensing data retrieval

REFERENCES

[1] King M.D., Strange M.G., Leone P., Blaine L.R., "Multiwavelength scanning radiometer for airborne measurements of scattered radiation within clouds", *J. Atmospheric and Oceanic Technology*, 1986, **3**, 513-522

[2] King M.D., "Directional and spectral reflectance of the Kuwait oil-fire smoke", *J. Geophysical Research*, 1992, **97**, D13, 14545-14549,

[3] Gatebe C.K., King M.D., Lyapustin A.I., Arnold G.T., Redemann J., "Airborne spectral measurements of ocean directional reflectance", *J. Atmospheric Sciences*, 2005, **62**, 1072-1092,

[4] Arnold G.T., Tsay S.C., King M.D., Li J.Y., Soulen P.F., "Airborne spectral measurements of surface-atmosphere anisotropy for arctic sea ice and tundra", *Int. J. Remote Sensing*, 2002, **23**, 18, 3763-3781,

[5] Gatebe C.K., King M.D., Platnick S., Arnold G.T., Vermote E.F., Schmid B., "Airborne spectral measurements of surface-atmosphere anisotropy for several surfaces and ecosystems over southern Africa", *J. Geophysical Research*, 2003, **108**, D13, 25-1-16,

[6] Bruegge C.J., Stiegman A.E., Rainen R.A., Springsteen A.W., "Use of Spectralon as a diffuse reflectance standard for in-flight calibration of earth-orbiting sensors", *Optical Engineering*, 1993, **32**, 805-814,

[7] Oren M., Nayar S.K., "Generalization of the Lambertian model and implications for machine vision", *International Journal of Computer Vision*, 1995, **14**, 227-251,

[8] Schlick C., "An inexpensive BRDF model for physically-based rendering", Eurographics '94, 1994, **16**, 233-246,

[9] Gao F., Schaaf C.B., Strahler A.H., Jin Y., Li X., "Detecting vegetation structure using a kernel-based BRDF model", *Remote Sensing of Environment*, 2003, **86**, 198-205,

[10] Proctor J.R., Barnes P.Y., "NIST High accuracy reference reflectometer - spectrophotometer", *J. Res. Nat. Inst. Stand. Technol.*, 1996, **101**, 619-627,

[11] Nicodemus F.E., Richmond J.C., Hsia J.J., Ginsburg I.W., Limperis T., "Geometrical considerations and nomenclature for reflectance", *National Bureau of Standards, NBS monograph 160*, Oct. 1977,

[12] Stover J.C., "Optical scattering: measurement and analysis", SPIE Press, Bellingham, Washington, 1995,

[13] Schiff T.F., Knighton M.W., Wilson D.J., Cady F.M., Stover J.C., Butler J.J., "A design review of a high accuracy UV to near infrared scatterometer", Proc. SPIE, 1993, **1995**, 121-130,

[14] Taylor B.N., Kuyatt C. E., "A guidelines for evaluating and expressing the uncertainty of NIST measurement results", NIST Technical Note 1297, U.S. Department of Commerce, National Institute of Standards and Technology, Sep. 1997,

[15] Early E.A., Barnes P.Y., Johnson B.C., Butler J.J., Bruegge C.J., Biggar S.F., Spyak P.S., Pavlov M.M., "Bidirectional reflectance round-robin in support of the Earth observing system program", *J. Atmospheric and Oceanic Technology*, 2000, **17**, 1077-1091,

[16] Georgiev G.T., Butler J.J., "Bidirectional reflectance distribution function and directional-hemispherical reflectance of a Martian regolith simulant", *Optical Engineering*, 2005, **44**, 036202-1-11,

[17] Vermote E.F., Tanré D., Deuzé J.L., Herman M., Morcrette J.J., "Second simulation of the satellite signal in the solar spectrum, 6S: An overview", *IEEE Trans. Geosci. Remote Sens.*, 1997, **35**, 675-686.